JJEE

Volume 11| Number 4 | Pages 758-775

Jordan Journal of Electrical Engineering

ISSN (print): 2409-9600, ISSN (online): 2409-9619

Homepage: jjee.ttu.edu.jo

Synergistic Control of High-Performance GPV Systems: Integrating Bio-inspired CS MPPT, SVPWM-CDSC for Maximizing PV Power Extraction and Grid Resilience

Muhammad Hafeez Mohamed Hariri[1*]

[1] Universiti Sains Malaysia, Malaysia
E-mail: muhammadhafeez@usm.my

Received: Sep 30, 2025 *Revised: Oct 31, 2025* *Accepted: Nov 14, 2025* *Available online: Jan 20,2026*

***Abstract*—** The rapid expansion of renewable energy systems has positioned grid-connected photovoltaic generation systems at the forefront of sustainable electricity production. Despite their potential, these systems face technical challenges such as efficient power extraction under varying atmospheric conditions and reliable synchronization with the utility grid during disturbances. This research presents a comprehensive performance analysis of a two-stage three-phase GPV system incorporating a Cuckoo Search-based Maximum Power Point Tracking algorithm, a DC-DC boost converter, a Space Vector Pulse Width Modulation, LCL filters, and a CDSC grid synchronization mechanism. The switching sequence generated by Space Vector Pulse Width Modulation minimizes harmonic distortion, maximizes voltage utilization, and improves synchronization with the utility grid, resulting in better overall system performance. The proposed architecture has achieved a maximum power transfer of 108.3kW, MPPT tracking efficiency of 96.15%, and generates low total harmonic distortions of 2.06%. The outcomes demonstrate that the proposed system performs efficiently, produces high-quality power, and integrates well with the grid even during disturbances, making it both economically and technically viable for large-scale as well as industrial use.

***Keywords*—** CDSC synchronization; Cuckoo Search MPPT; LCL filter; SVPWM inverter; Photovoltaic.

Nomenclature

AC	Alternating Current	MCA	Musical Chairs Algorithm
BPF	Band-pass Filter	MPA	Marine Predator Algorithm
CCM	Continuous Conduction Mode	MPP	Maximum Power Point
CRC	Current Reference Calculation	MPPT	Maximum Power Point Tracking
CS	Cuckoo Search	PF/p.f.	Power Factor
CDSC	Cascaded Delay Signal Cancellation	PI	Proportional–Integral
D	Duty Cycle	PO	Perturb and Observe
DC	Direct Current	PLL	Phase Locked Loop
DSOGI	Double Second Order Generalized Integrator	PV	Photovoltaic
ESR	Equivalent Series Resistance	PVSC	PV-side Converter
FO	Fractional Order	PWM	Pulse Width Modulation
FOBC	Fifth-Order Boost Converter	RMS	Root Mean Square
FOPI	Fractional Order Proportional–Integral	SMC	Sliding Mode Control

* Corresponding author

DOI: https://doi.org/10.5455/jjee.204-1759219278

FOPIT	Fractional Order Proportional–Integral-Tilt	SPWM	Sinusoidal Pulse Width Modulation
GPV	Grid-Connected Photovoltaic	SRF	Synchronous Reference Frame
INC	Incremental Conductance	SVPWM	Space Vector Pulse Width Modulation
ISMC	Integral Sliding Mode Control	THD	Total Harmonic Distortion
LCL	Inductor-Capacitor-Inductor	VSI	Voltage Source Inverter

1. INTRODUCTION

The growing worldwide need for environmentally friendly and renewable power sources has spurred faster integration of solar energy (photovoltaic) technology [1, 2]. Grid-connected PV (GPV) generation systems, in particular, are seen as pivotal in the transition toward green energy due to their ability to directly convert solar power into usable electrical energy [3-5]. Nevertheless, the effectiveness of these systems is heavily reliant on environmental conditions, particularly the intensity of sunlight (solar irradiance) and the temperature of the PV modules [6, 7]. Additionally, the inherent DC nature of PV output necessitates effective power conversion and synchronization mechanisms for seamless grid integration. Challenges in GPV systems include suboptimal power extraction due to deviation from the Maximum Power Point (MPP), quality deterioration in injected power, and poor synchronization under grid disturbances [8-10].

Contrary to a single-phase system, the three-phase GPV generation system is commonly preferred in high-powered applications as its ability to provide almost constant power flow and can avoid excessive asymmetry in the grid current [11, 12]. The use of conventional MPPT techniques resulted in the PV operating point oscillating in the vicinity of the MPP, thereby wasting energy [13]. According to the literature, most existing GPV systems use a SPWM switching topology, which results in high harmonic content, especially in the injected current waveform from the inverter section to the utility grid. A more advanced switching method, such as SVPWM, is a superior choice for the inverter switching [14].

Moreover, the existing grid synchronization mechanisms based on the popular PLL method experience difficulties in providing accurate grid information, particularly during unpredictable atmospheric profiles as well as various grid disturbances [15].

The maximum power transfer is the utmost objective regarding developing the GPV generation system. The system response towards the transient conditions on the grid-connected inverter due to the presence of different types of faults, such as voltage unbalance, voltage dip, high harmonic distortions, and various line faults in the grid power line, also becomes another concern in assessing the ability, as well as the overall performance of designated local controllers to compensate for the changes.

This research addresses these issues by proposing an enhanced system architecture optimized for maximum power transfer and grid reliability. The proposed enhancement scheme tailor's subsystem components to address the key challenges PV researchers typically face when building an efficient GPV generation system.

Table 1 summarizes various studies related to GPV systems, detailing their components, control strategies, and main contributions.

Table 1. Summary of recent grid-connected PV system studies.

Ref.	First Stage	Second Stage	MPPT	DC Link	Modulation Technique	Synchronization Scheme	Contribution
[16]	Boost	VSI	MPA	FOPIT-FOPI	SPWM	PLL	Merge the features of cascaded control and FO control
[17]	Boost	VSI	INC	FOBC-PVSC	SPWM	BPF	Evaluates the stability of the FOBC-PVSC under different input capacitor values and grid conditions
[18]	Boost	VSI	INC	PI	SPWM	Backstepping-sliding mode	Introduce the hybrid Backstepping-sliding mode technique
[19]	Boost	VSI	INC	PI	SPWM	PLL	Proposes a Low-Voltage Ride-Through control strategy
[20]	Boost	VSI	PO	PI	SPWM	PLL	Proposes (CRC) methods for the PV system under unbalanced grid voltage fault.
[21]	Boost	VSI	INC	PI	SPWM	PLL	Introduce a robust μ value control method based on the hybrid sensitivity theory

This research proposed contributions to the design and enhancement of two-stage three-phase GPV systems. Specifically, the paper utilizes a sophisticated MPPT algorithm based on the CS method to maximize power generation despite changes in weather conditions. The effective integration of SVPWM within the system architecture further enhances the effectiveness of the proposed system. The role of the two-stage conversion process, with an emphasis on the selection of the DC-DC boost converter and its interaction with the voltage source inverter. Moreover, the switching sequence generated by SVPWM ensures minimal harmonic distortion, higher voltage utilization, and improved synchronization with the utility grid, leading to better overall system performance, particularly under varying atmospheric conditions and grid disturbances. Additionally, a CDSC synchronization mechanism is implemented to further enhance the control, reliability, and efficiency of grid synchronization, even during grid disturbances.

2. RESEARCH DESIGN FRAMEWORK

The proposed system incorporates several advanced sub-components designed to maximize energy conversion efficiency while ensuring reliable integration with the utility grid. The system utilizes a CS MPPT method, which optimally adjusts the operation of the photovoltaic array to extract the maximum available power under varying environmental conditions. A conventional DC-DC boost converter is employed to regulate the DC voltage from the PV array, ensuring that the DC input to the three-phase inverter remains within the optimal range. The three-phase VSI, controlled by SVPWM switching sequence, is responsible for converting the DC power into high-quality AC power suitable for grid injection. To

minimize harmonic distortion, an LCL filter configuration is used, significantly improving the power quality and meeting the required grid standards [22]. A CDSC scheme ensures robust synchronization with the utility grid, enabling stable operation even during grid disturbances or fault conditions [23]. This configuration is chosen for its ability to extract and convert solar energy while maintaining compliance with grid codes and ensuring a seamless, fault-tolerant integration with the electrical grid. The structural components of the suggested three-phase GPV system are shown in detail in Fig. 1. The circuit architecture is made of PV arrays, a DC-DC Boost converter, and a three-phase inverter within the power circuitry. Meanwhile, the supervisor controller is made of an MPPT algorithm block, switching techniques, as well as a grid synchronization controller block.

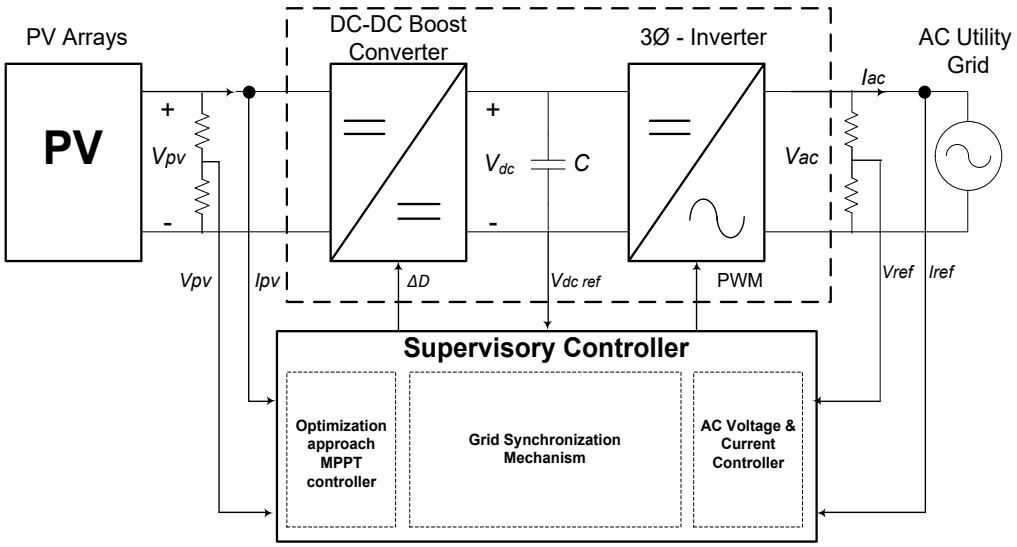

Fig. 1. Overall block diagram of the GPV generation system.

2.1. Maximum Power Point Tracking (MPPT)

The CS algorithm is a nature-based metaheuristic strategy derived from observing the parasitic egg-laying behaviour of cuckoo birds. In this system, CS is employed for real-time tracking of the MPP under variable atmospheric conditions. Unlike conventional methods, CS offers faster convergence, reduced oscillations, and better adaptability to rapid changes in irradiance and temperature [24]. The general equation for CS is given as follows [25];

$$X_i^{t+1} = X_i^t + \alpha \oplus Levy(\lambda) \tag{1}$$

$$\alpha = \alpha_o\left(X_i^t - X_{opt}\right) \tag{2}$$

$$Levy(\lambda) = \frac{u}{|v|} \tag{3}$$

$$\emptyset_u = \left(\frac{\Gamma(\lambda)\sin\left(\frac{\pi(\lambda-1)}{2}\right)}{\Gamma\left(\frac{(\lambda)}{2}\right)(\lambda-1)2^{\frac{(\lambda-2)}{2}}}\right)^{\frac{1}{(\lambda-1)}} \tag{4}$$

From the above-listed equations, i is denoted as the number of the nest position in the t iteration, the constant X_i^{t+1} represent the new solutions generated at $t+1$, α indicates the step size, the term X_{opt} represent the current optimal solution, $Levy(\lambda)$ is a random search vector in which the parameter varied between the values of 1 and 3, which was generated by the Levy flight, in which the notation $u \sim N(0, \delta_U^2)$ is defined as the random displacement in the x-direction and $v \sim N(0,1)$ is the random displacement in the y-direction respectively. The detection step $\emptyset_u$ is the initialization value when a certain event should occur.

2.2. DC-DC Boost Converter

A DC-DC boost converter is utilized to regulate the PV output voltage, ensuring optimal input to the inverter. The resulting mathematical equation expresses the output voltage, V_o in terms of input voltage, V_i and the duty cycle ratio, D is given as follows,

$$V_o = \frac{V_i}{1-D} \quad , for \ 0 < D < 1 \tag{5}$$

To ensure the inductor current I_L and capacitor voltage V_C operate in CCM, several criteria must be met. According to [26], determining the DC-DC boost converter's power stage requires specific design parameters. The process for specifying the DC-DC boost converter generally begins with selecting the inductor capacity (L), as outlined in Eq. (6),

$$L = \frac{V_i*(V_o-V_i)}{\Delta I_L*f_s*V_o} \tag{6}$$

Moreover, the following equation mathematically defines the inductor ripple current ΔI_L, where the value of the constant X, is ranged between $0.2 \ to \ 0.4$.

$$\Delta I_L = X * I_{o\,max} * \frac{V_o}{V_i} \tag{7}$$

The expression for the minimum output capacitance, $C_{o\,min}$ required for the output capacitor is given by,

$$C_{o\,min} = \frac{I_{o\,max}*D}{f_s*\Delta V_o} \tag{8}$$

and given,

$$\Delta V_o = ESR * \left(\frac{I_{o\,max}}{1-D} + \frac{\Delta I_L}{2}\right), ESR = 1.5\Omega \tag{9}$$

where the notation of f_s, $I_{o\,max}$, ΔV_o and ESR stands for DC-DC Boost converter's frequency switching, maximum output current, output voltage ripple, and the amount of allowable output capacitor equivalent series resistance, respectively [27].

2.3. Three-phase Voltage Source Inverter

In this research, the 180° conduction mode is chosen due to its enhanced efficiency in using the switching components [28]. Subsequently, the relationship between the VSI's RMS line voltage, V_{Line} and the DC-DC boost converter's input DC voltage, V_{dc} is provided by Eq. (10) [29],

$$V_{Line} = m_a \frac{\sqrt{3}}{2\sqrt{2}} V_{dc} \tag{10}$$

where m_a is denoted as the modulation index. Eq. (11) provides the formula used to calculate the Total Harmonic Distortion (THD) for either the voltage or the current.

$$THD = \sqrt{\sum_{n=2}^{\infty} \left(\frac{M_{n\,rms}}{M_{1\,rms}}\right)^2} * 100 \tag{11}$$

where $M_n \ rms$ is the Root Mean Square (RMS) value of the harmonic component for a given quantity (either voltage or current), represented by n^{th}. Separately, the system's efficiency (η) can be determined as:

$$Efficiency, \eta = \frac{Output \ power, P_o}{Input \ power, P_i} * 100 \ (\%) \tag{12}$$

2.4. Space Vector Pulse-Width Modulation Technique

The SVPWM technique for a three-phase VSI is based on transforming the three-phase signals (a, b, c) into their equivalent vector representation in the two-dimensional (d, q) plane.

The switching time durations for the SVPWM within any given sector can be calculated using the relationships provided in Eqs. (13)-(15).

$$T_1 = \frac{\sqrt{3}*T_z*|V_{ref}|}{V_{dc}}\left(\sin\frac{n}{3}\pi\cos\alpha - \cos\frac{n}{3}\pi\sin\alpha\right) \quad (13)$$

$$T_2 = \frac{\sqrt{3}*T_z*|V_{ref}|}{V_{dc}}\left(-\cos\alpha * \sin\frac{n-1}{3}\pi + \sin\alpha * \cos\frac{n-1}{3}\pi\right) \quad (14)$$

$$T_0 = T_Z - T_1 - T_2 \quad (15)$$

where $|V_{ref}|$, n, α, T_0, T_1, T_2 and T_Z are denoted as the magnitude of the reference voltage vector, the sector number, the angle between these two adjacent vectors, the total duration for the zero-voltage vectors, the switching durations for the two active voltage vectors adjacent to the reference vector, and the total sampling period, respectively.

2.5. Grid Synchronization Mechanism

The amplitude, phase angle, and phase sequence of the three-phase VSI's voltage waveform are vital properties that govern proper PV system synchronization with the electrical grid [30], [31]. Once the PV-grid synchronization has taken place, then the current from the three-phase VSI can be injected into the utility grid. The complex power is given by;

$$S = I^* * V_{inv} \quad (16)$$

$$S = \left[\frac{|V_{inv}|\angle\delta - |V_{grid}|\angle 0}{|Z_t|\angle\gamma}\right]^* * V_{inv} \quad (17)$$

$$S = \frac{[V_{inv}]^2}{Z_t}\cos\gamma - \frac{|V_{inv}||V_{grid}|}{|Z_t|}\cos(\gamma+\delta) \quad (18)$$

Given that the transmission line's resistance is typically much smaller than its inductance, the link is often approximated as purely inductive, allowing γ to be assumed as 90°. By simplifying Eq. (16) until Eq. (18), the mathematical expression of the injected real power P and reactive power Q are given as follows,

$$P = \frac{|V_{inv}||V_{grid}|}{X_L}\sin\delta \quad (19)$$

$$Q = \frac{[V_{inv}]^2}{X_L} - \frac{|V_{inv}||V_{grid}|}{X_L}\cos\delta \quad (20)$$

where V_{inv} , I^*, δ, V_{grid}, Z_t, γ, P, Q and X_L denotes as inverter's voltage, injected current, phase angle, grid's voltage, total impedance, phase angle, real power, reactive power, and the load of the line impedance, respectively [32]. Meanwhile, the development of CDSC grid synchronization stems from the limitation that both traditional PLLs and DSOGIs struggle to maintain accurate phase and frequency tracking when the line grid voltage is severely distorted or contains DC offset components. The configuration of the CDSC block when integrated with an SRF-PLL is illustrated in Fig. 2.

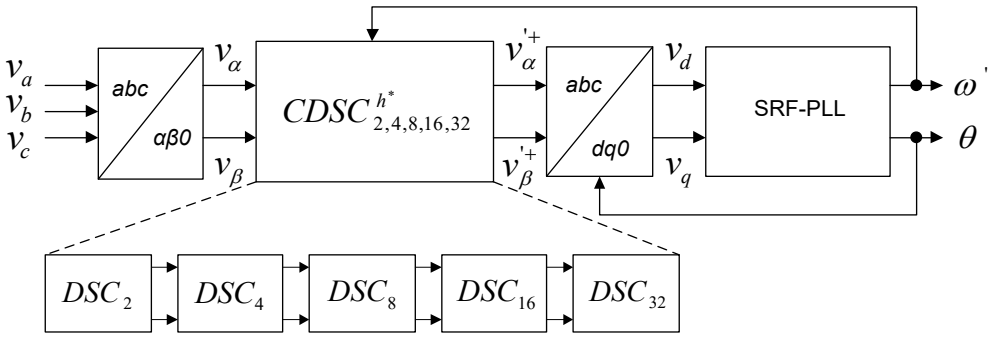

Fig. 2. CDSC module with transformation block [33].

The various design specifications chosen for the suggested two-stage three-phase GPV generation system are presented in Table 2. Based on the proposed system rating and selected parameters, the overall simulation circuit has been constructed accordingly in MATLAB-Simulink (MATLAB 2018b) environments.

Table 2. The overall list of parameters for the proposed three-phase GPV System.

Section	Parameter	Value
PV Modules	Reference Model	1Soltech 1STH-215-P
	Nominal peak power, P_{max}	$213.15W$
	The voltage at maximum power, V_{mp}	$29V$
	Current at maximum power, I_{mp}	$7.35A$
	Short-circuit current, I_{sc}	$7.84A$
	Open-circuit voltage, V_{oc}	$36.3V$
	PV modules in series, n_s	10
	PV modules in parallel, n_p	47
DC-DC boost converter	Rated Power, P	$100kW$
	Input voltage, V_i	$250V_{DC} - 350V_{DC}$
	Boost Inductor, L_b	$1.45mH$
	Switching frequency, f_s	$5kHz$
	Boost Input Capacitor, C_i	$220uF$
	Boost Output Capacitor, C_b	$3227uF$
	Output voltage, V_{dc}	$600V_{DC}$
Three-phase VSI	Modulation Index, m_a	1
	Switching frequency, f_s	$10kHz$
	PWM Technique	$SPWM$
	Output Phase Voltage, $V_{o\ rms}$	$230V_{LN}$
Line Filters	Line Inductance, L_f	$500uH$
	Line Capacitance, C_f	$100.28uF$
Three-phase utility grid	Power Rating	$10000VA$
	Operating Line Voltage, V_{grid}	$400V_{LL}$
	Operating line frequency, f	$50Hz$

3. RESULTS AND DISCUSSION

For this research, the 1Soltech (1STH-215-P) PV module was selected as the standard model. According to its specifications, the Maximum Power Point Voltage (V_{mpp}) is 29V, and the Maximum Power Point Current (I_{mpp}) is 7.35A. Consequently, the Maximum Power Rating $(P_{mpp})$for a single module is calculated as 213.15W (29V×7.35A).

The research maintains the surface temperature (T) at a constant $25°C$ since temperature changes have a minimal impact on the resulting PV current. The goal is to design the PV arrays to generate a total real power (P) of 100kW. To achieve this, the system requires 47 parallel strings and 10 PV modules in series per string.

The PV arrays are evaluated under three distinct solar irradiations (G) levels: $1000W/m^2$, $600W/m^2$, and $200W/m^2$. The resulting Current-Voltage $(I-V)$ and Power-Voltage $(P-V)$ characteristic curves of the PV arrays for these specified irradiation levels are depicted in Fig. 3.

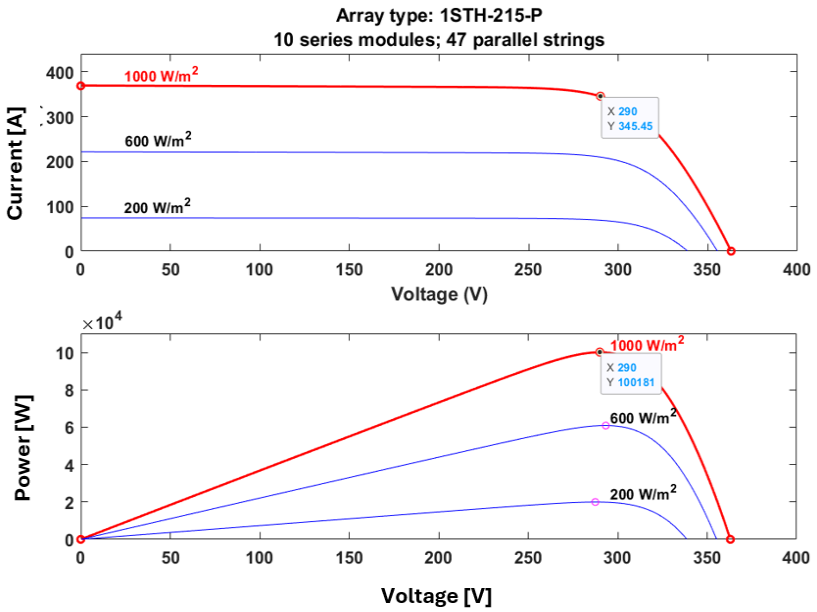

Fig. 3. The PV characteristics of $I-V$ and the $P-V$ at different irradiation levels.

Based on the generated current waveform corresponding to the PWM signal, as illustrated in Fig. 4, the inductor current, I_{ind} is believed to have been working in continuous conduction mode (CCM). The average value of I_{ind} at the duty cycle, $D = 0.5$ and with the output DC voltage of $600V$ is approximately $325A$. The DC-DC boost converter has been designed in such a way that it can withstand the DC voltage and current level of the PV system for a power rating of $100kW$.

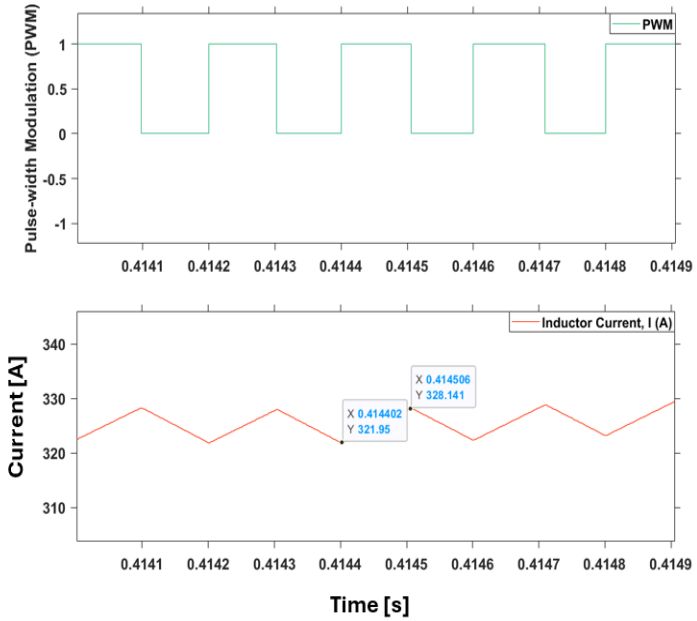

Fig. 4. The generated inductor current waveform of the DC-DC boost converter.

As for the benchmarking purpose, the typical PO MPPT technique is the first to be used in this research analysis. To examine the tracking effectiveness of the PO MPPT method, the PV arrays were assessed using three varying intensities of solar irradiation, which can be further characterized as uniformly distributed, gradually and suddenly changing of atmospheric conditions as illustrated in Fig. 5. The performance of the PO MPPT tracking response can be observed by the magnitude of PV power oscillation and also the amplitude variation of the duty cycle, D.

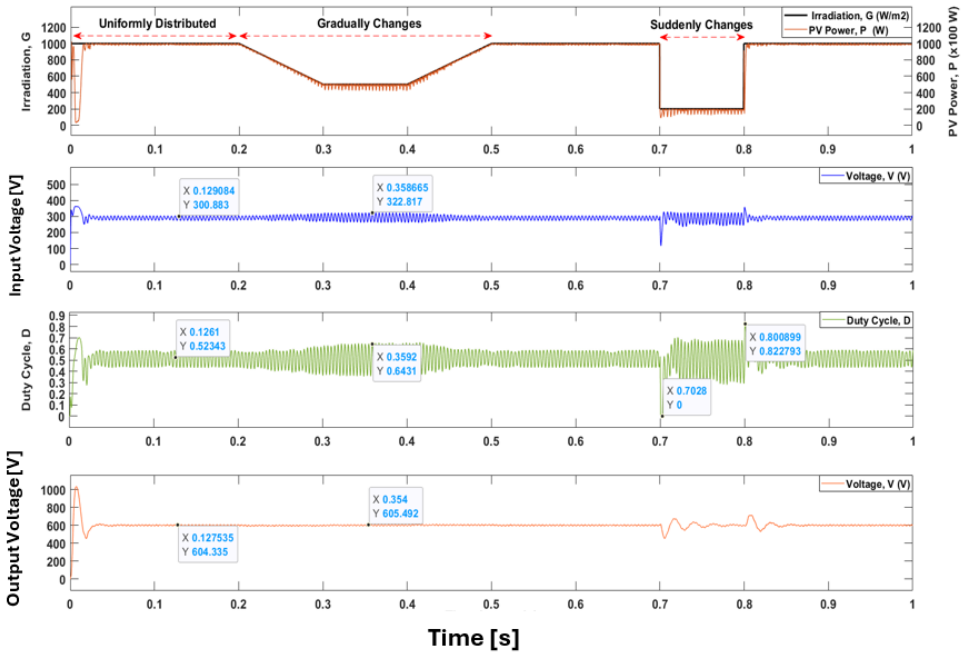

Fig. 5. The generated PV power, P and the variation of duty cycle, D over time using the PO MPPT method.

The next MPPT method investigated in this research is incremental conductance or INC. Among all the conventional MPPTs available in the literature, the INC is the most preferable MPPT method used to extract the maximum available power from the PV arrays. As illustrated in Fig. 6, with the identical atmospheric profile applied, the equivalent PV power, P, and duty cycle, D is generated. The oscillation of the generated power of PV arrays and the variation of D for the INC method is slightly less compared to the previous PO MPPT method. The highest amplitude deviation of D ever recorded is 0.6. This maximum deviation of D occurred during the sudden changes of atmospheric conditions (G) from the value of $1000W/m^2$ and drops to the irradiation level of $200W/m^2$.

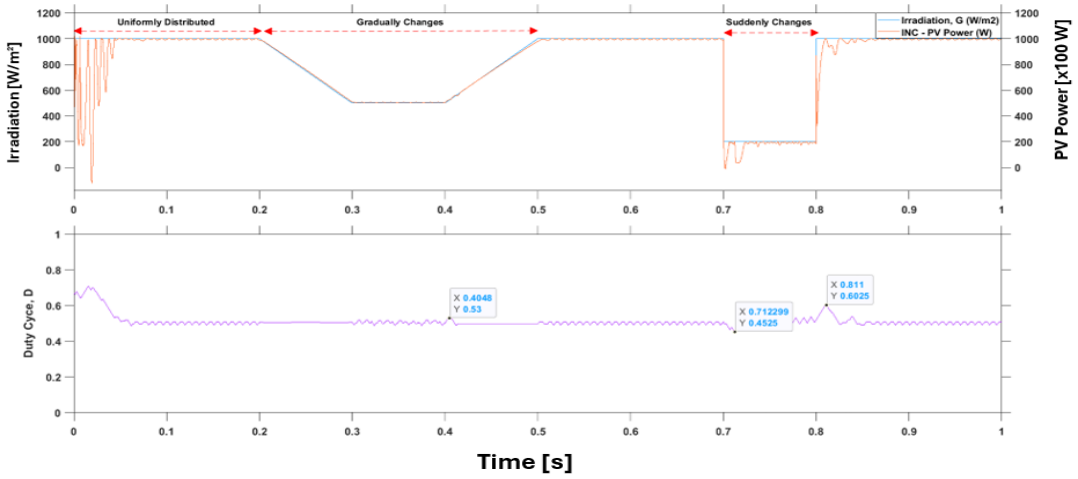

Fig. 6. The generated PV power, P and the variation of the duty cycle, D over time using the INC MPPT method.

In the meantime, the CS technique is categorized as one of the latest and advanced distinctive meta-heuristic optimization algorithms to be applied to track the PV maximum power point or MPP. As illustrated in Fig. 7, it produces crystal clear and much better-quality results in terms of PV power oscillation as well as very low amplitude variation of D. It produces almost no PV power oscillation at all, and the value of D is consistently kept at a value near 0.5 even in the event of fluctuating atmospheric conditions.

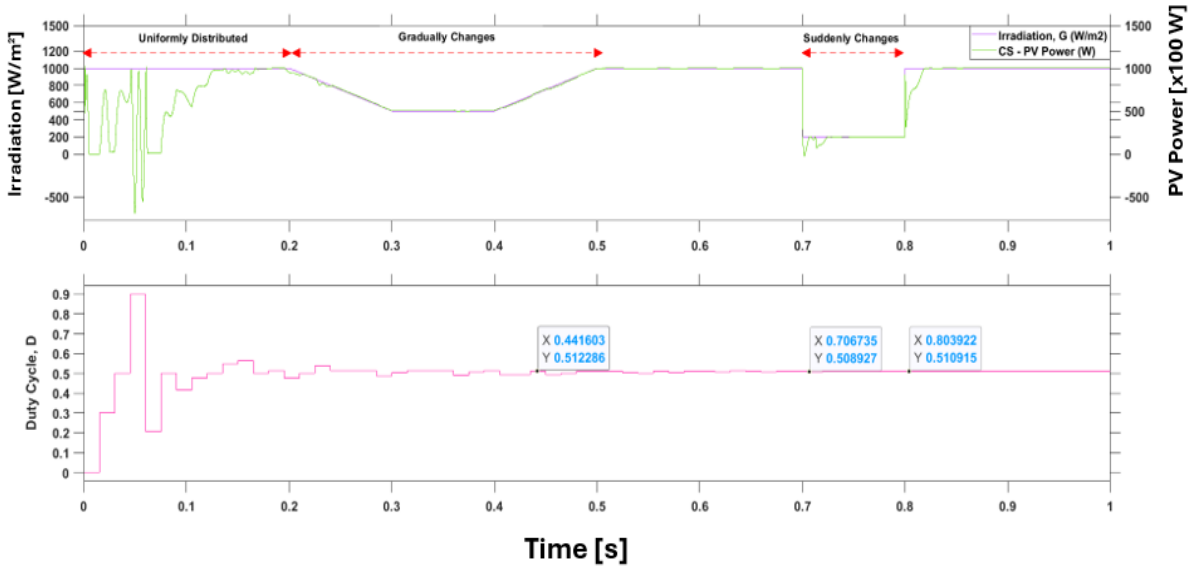

Fig. 7. The generated PV power, P and the variation of the duty cycle, D over time using the CS MPPT method.

Furthermore, Fig. 8 shows the output voltage waveform produced by the three-phase inverter before and after the LCL filters. The recorded RMS value of the generated inverter's phase voltage waveform is $230V_{rms}$ with $50Hz$ operating line frequency. The peak RMS value of the generated inverter phase voltage waveform is $325.27V$. The generated inverter's voltage waveforms after the LCL filters are purely sinusoidal, as this is one of the prerequisite conditions before being synchronized to the utility grid.

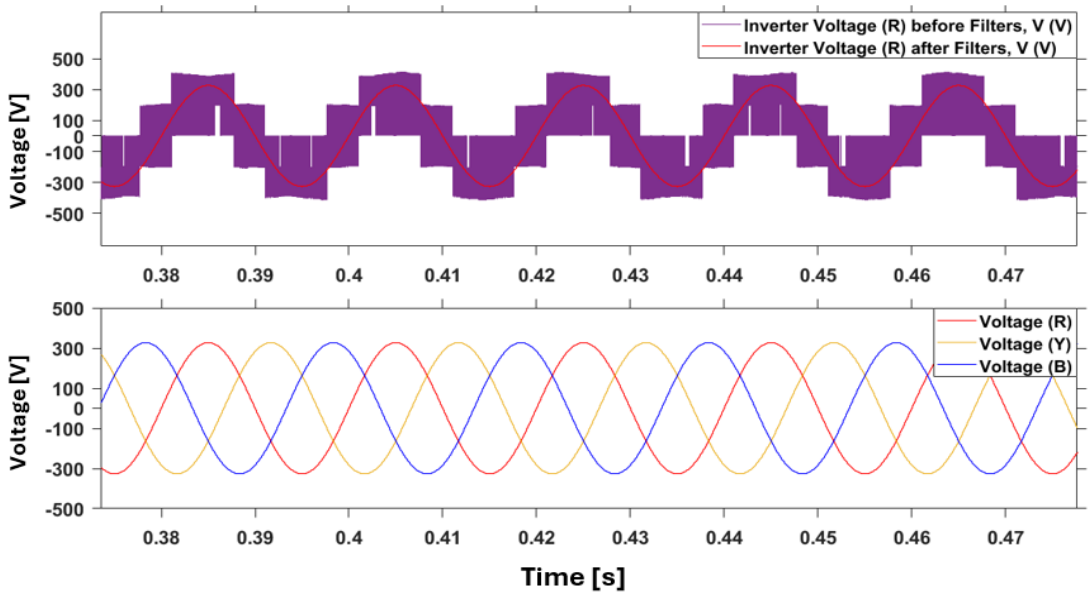

Fig. 8. The inverter voltage waveform profile before and after the LCL filters.

The reference switching patterns of the SVPWM technique are illustrated in Fig. 9. The line frequency of the voltage waveform is kept at 50Hz with the modulation index (m_a) is set at a value of 1.0.

Moreover, as shown in Fig. 10, in SRF, the alpha, V_α and beta voltage, V_β components of the grid voltages are separated by 180° electrical degrees with the amplitude voltage value of $326V$. A phase-locked loop (PLL) controller tracks the line frequency effectively as the operating line frequency, f is kept at $50Hz$ for every complete cycle of each $\alpha\beta$ voltage component.

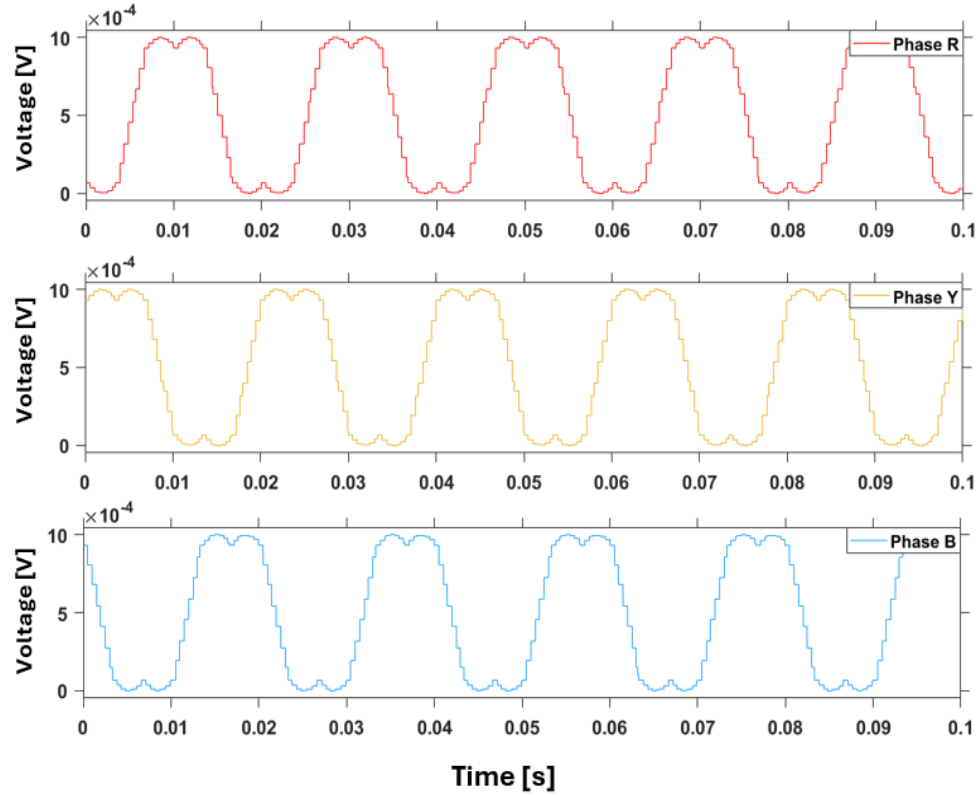

Fig. 9. The reference voltage waveforms generated using SVPWM.

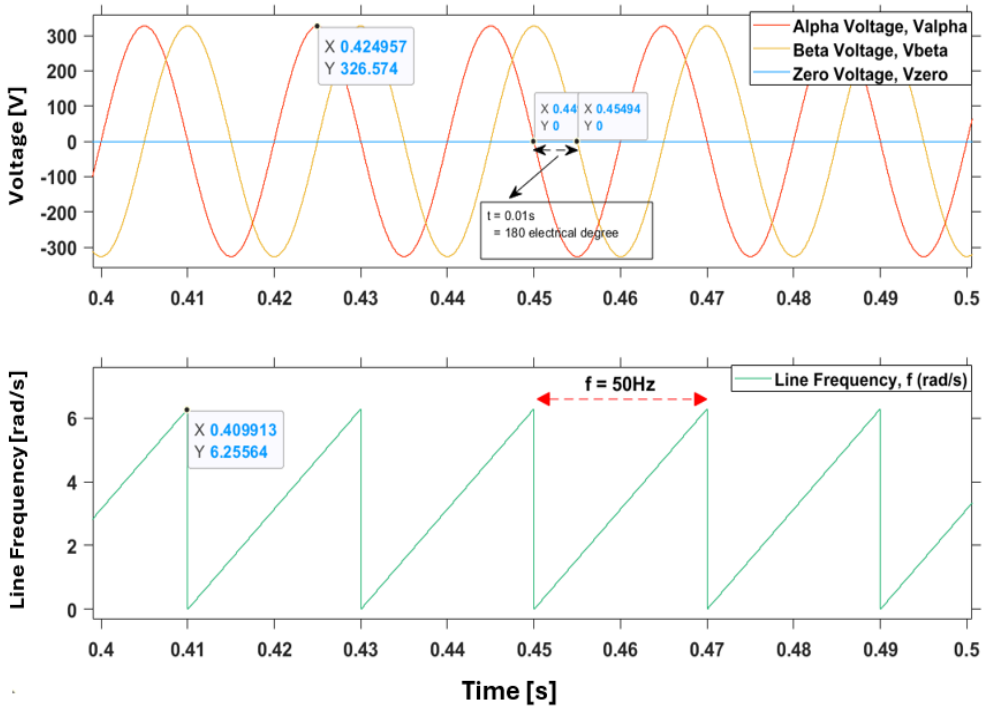

Fig. 10. Performance of line frequency, f with respect to the voltage waveform in the $\alpha\beta$ reference plane.

As displayed in Fig. 11, the direct voltage component, V_d is measured at $326V_{dc}$. On the other hand, the reactive voltage component, denoted as V_q is kept at zero value since there is no reactive power that has been controlled.

Meanwhile, the direct, I_d and quadrature, I_q components of the inverter line currents precisely follow the designated reference current waveform components. The performance of the designated current controller during the steady-state conditions is shown in Fig. 12.

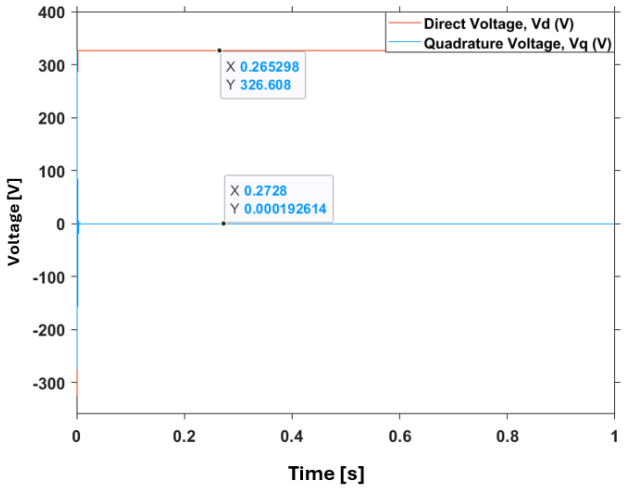

Fig. 11. The direct, V_d and quadrature, V_q components of line voltage.

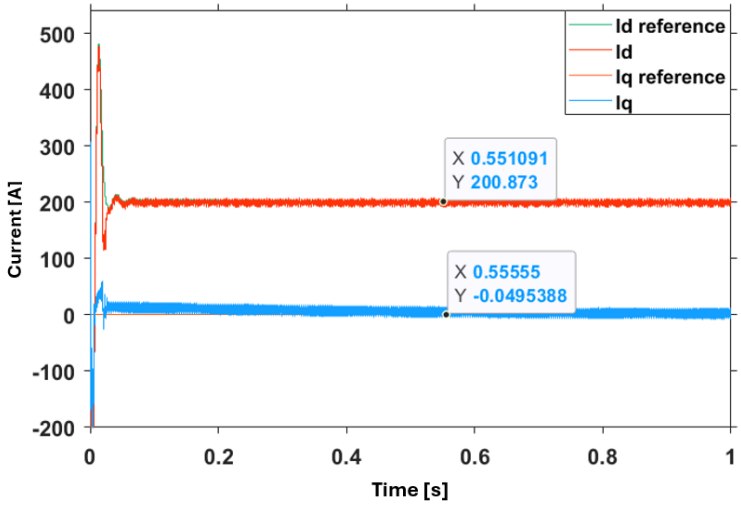

Fig. 12. The I_d and I_q components of the inverter line current in dq reference plane.

In Fig. 13, the grid voltage reaches a peak amplitude of 325V, and the injected current waveform's peak amplitude is 200A. Crucially, it shows that the injected current waveform is perfectly aligned with the grid voltage waveform. This precise phase synchronization occurs as the system achieves a power factor or $p.f$ that is nearly unity (≈1).

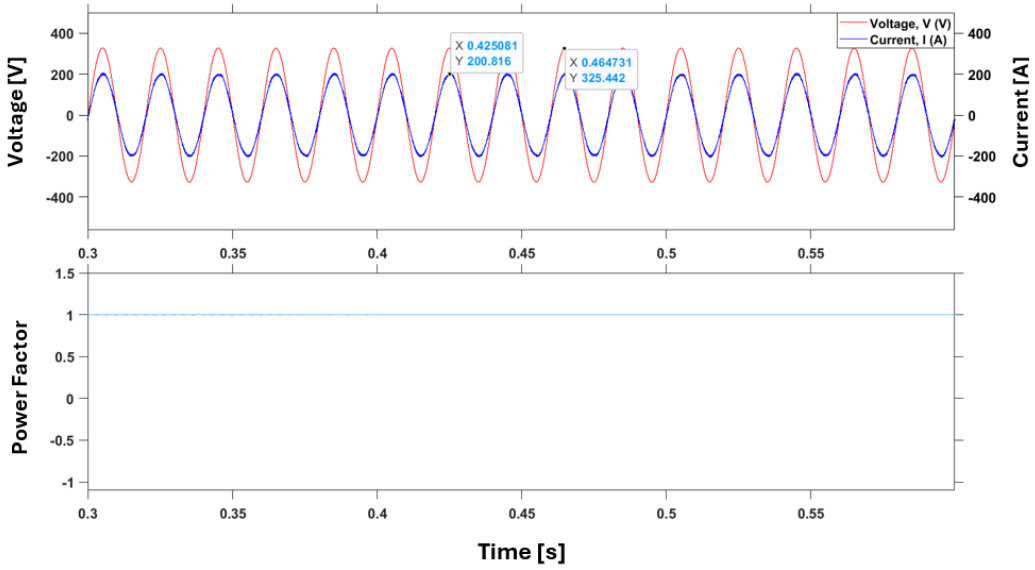

Fig. 13. The grid voltage and injected current waveform are in-phase, and the corresponding value of $p.f$.

As illustrated in Fig. 14, the injected active power, P at a uniform irradiation level of $1000W/m^2$ is approximately $100kW$ as per design rating, whereas the value of reactive power, Q is kept near-zero value. The value of injected real power, P remains constant as there are no changes in terms of irradiation and temperature readings on the PV system side. Meanwhile, the phase difference between the inverter voltage waveform and the reference waveform of the grid voltage is measured at approximately 11° displacement.

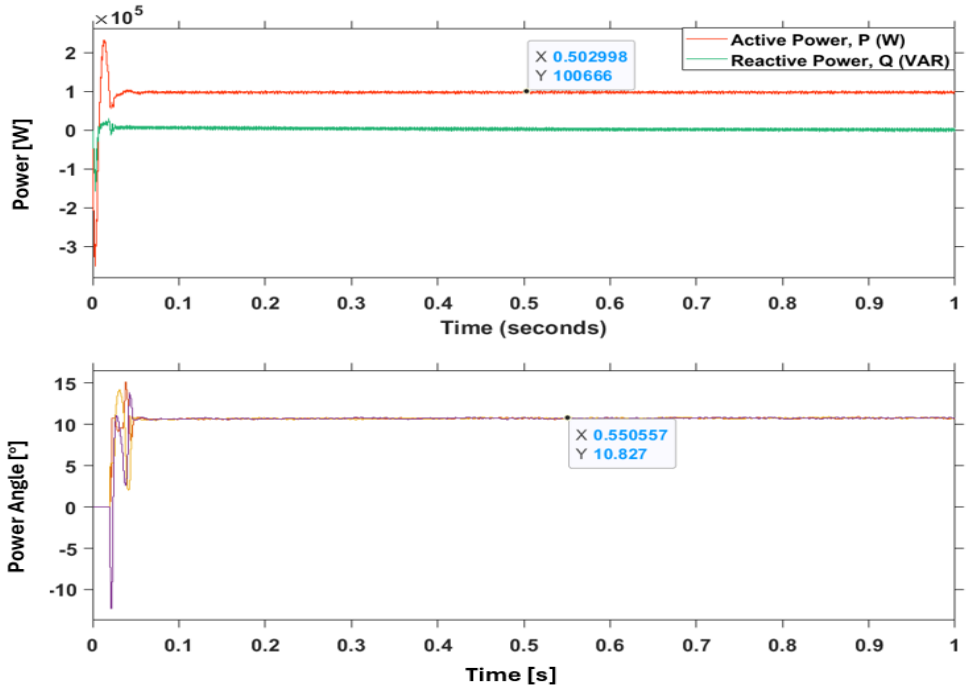

Fig. 14. Relationship between the injected real power, P and the phase difference, δ.

Based on the literature [34], one of the main criteria to perform effective PV-grid synchronization is to have a matching voltage waveform profile in terms of amplitude, operating line frequency, and phase sequence. The generated inverter's phase voltage waveform is not in a fully sinusoidal form, and it contains a high value of THD due to the power switching effect that took place beforehand. This kind of waveform profile is not acceptable for grid synchronization, as it may cause the controller to malfunction in which may lead to the damage of electrical as well as electronic equipment and create a high potential of safety hazards to the personnel in charge. Therefore, based on the parameters designed as described earlier, the LCL passive filter configuration is specifically connected at the grid-connected side. This approach is to reduce the content of voltage as well as the current harmonics generated from the switching process of the three-phase VSI within the permissible standard limit. It is well-known that the harmonic content of voltage waveforms is not significant since it has already been synchronized with the grid voltage, where it is defined as an infinite source. To replicate one scenario of the grid fault conditions, the THD of 70.71% is injected into the utility voltage grid as shown in Fig. 15. The THD distortions are initiated at $t = 0.3\ second$ until $t = 0.4\ second$. The THD generation is based on the order, the amplitude variation of the voltage waveform, the deviation of phase angle, and lastly the sequence tousled. The respective profile of injected current waveforms that contain a high degree of THD_i is shown in the second row of the referenced figure. Even though the THD is terminated at $t = 0.4\ second$, still, some swinging occurred in the current waveform due to controller

action, which required some time to compensate for the changes. Among grid synchronization techniques, the PLL is the most widely recognized due to its simplicity. Additionally, methods such as DSOGI and CDSC further enhance the accuracy and reliability of synchronization, making it interesting to identify the single most suitable technique for the proposed system.

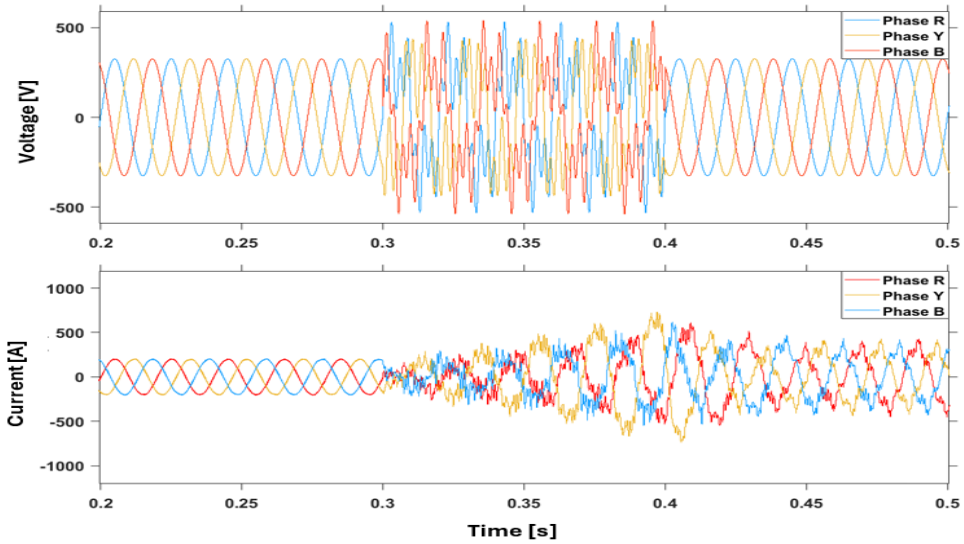

Fig. 15. The profile of grid parameters during harmonic distortion events.

By referring to Fig. 16, a noticeable oscillation in line frequency can only be seen occurring on the PLL method as it is directly affected by its phase angle tracking performance in the case where the grid voltage waveform was placed under harmonic distortion conditions. Meanwhile, the operating line frequency for DSOGI and CDSC is kept constant at $50Hz$. The controller performance of DSOGI and CDSC has shown better performance compared to the conventional PLL in the presence of harmonic distortions as there is no oscillation, and also no line frequency fluctuations have been observed over time.

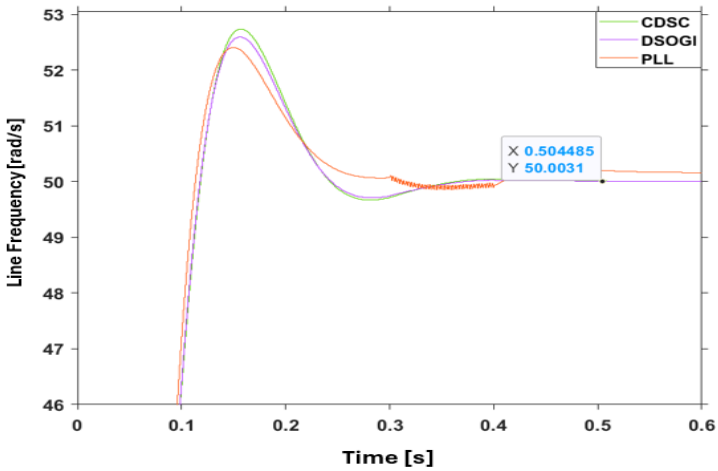

Fig. 16. The frequency tracking performance of the selected synchronization techniques under harmonic distortion conditions.

Then, the CDSC method has been identified as the most effective synchronization scheme, demonstrating near immunity to various types of grid disturbances. The DSOGI ranks second in performance; however, it struggles to accurately track the grid frequency under conditions of high THD. PLL, while less robust, remains functional under moderately distorted grid conditions. A comparative analysis of these synchronization techniques is presented in Table 3.

Table 3. Comparative analysis among synchronization schemes under grid fault conditions.

Types of grid faults	Grid Synchronization Schemes								
	PLL			DSOGI			CDSC		
	Performance Parameters			Performance Parameters			Performance Parameters		
	Accuracy	Speed	Error	Accuracy	Speed	Error	Accuracy	Speed	Error
Voltage unbalance	Low	Slow	Large	High	Fast	Small	High	Fast	Small
Voltage Surge	High	Medium	Large	High	Medium	Large	High	Fast	Small
Voltage Dip	High	Medium	Large	High	Medium	Large	High	Fast	Small
Frequency Jump	High	Medium	Large	High	Medium	Large	High	Fast	Large
Phase Jump	High	Medium	Small	High	Medium	Large	High	Fast	Large
Harmonic Distortions	Low	Slow	Large	High	Fast	Small	High	Fast	Small
Line-to-Line	Low	Slow	Large	High	Fast	Large	High	Fast	Large
Line-to-Line-to-Ground	Low	Slow	Large	High	Fast	Large	High	Fast	Large
Line-to-Line-to-Line	High	Medium	Large	High	Fast	Large	High	Fast	Large

Table 4 offers a detailed performance comparison between the proposed GPV generation system with related studies.

Table 4. Performance comparison of the proposed system against related studies.

Section	Article #1 [35]	Article #2 [36]	Article #3 [37]	This study
Year Published	2024	2025	2025	est. 2026
Scope	Simulation	Simulation	Simulation	Simulation
System Rating	$1kW$	$50kW$	$100kW$	$100kW$
MPPT	PO	INC	MCA-SMC	CS
DC-DC Converter	DC-DC Boost	DC-DC Boost	DC-DC Boost	DC-DC Boost
DC-Link Controller	PI	FO-ISMC-PI	PI	PI
Three-phase Inverter	Two-Stage	Two-Stage	Two-Stage	Two-Stage
Switching Topologies for Inverter	SVPWM	SPWM	SPWM	SVPWM
Line Filters Configuration	LC	LCL	LCL	LCL
Synchronization Mechanism	PLL	PLL	PLL	CDSC
Efficiency of MPPT	Not provided	$\eta = 90\%$ and requires 0.4 $second$ to reach a steady state.	$\eta = 90\%$	$\eta = 96\%$ and requires $0.05s$ to reach a steady state.
Power Oscillation	Not provided	A noticeable PV power oscillation occurred	A noticeable PV power oscillation occurred	No PV power oscillation occurred.
THD_i	1.69%	1.05%	2.43%	2.06%
System's Conditions	Steady-state	Tested under varying irradiation levels and a single grid fault condition	Tested under varying irradiation levels	Tested under varying irradiation levels and various grid fault conditions

The results confirm that the proposed system represents the most effective structural arrangement for connecting the PV system to the utility grid. This is based on its demonstrated superior metrics, including MPPT efficiency of 96%, a fast steady-state response time of only 0.05 seconds, and a low current (THD_i) level of 2.06%, and its capacity to maintain efficient operation even when facing various grid fault conditions.

4. CONCLUSION

The enhanced two-stage three-phase GPV system architecture demonstrates significant improvement by achieving a maximum power transfer of 108.3kW, MPPT tracking efficiency of 96.15%, and generates low THD_i of 2.06%. The proposed system integrates a robust bio-inspired CS heuristic to maximize solar power extraction under dynamic atmospheric conditions. The subsequent DC-AC conversion stage, governed by SVPWM, substantially mitigates THD, thus enabling precise synchronization with the utility grid. CDSC synchronization mechanism provides system resilience and the necessary control authority by accurately detecting sequence components during adverse asymmetrical voltage faults and transient grid perturbations. Ultimately, this comprehensive synergy of intelligent optimization (CS-MPPT) and robust grid-responsive control (SVPWM and CDSC) validates a highly optimized and scalable solution, thus establishing a foundation for next-generation and high-performance solar energy integration into future smart grids.

Acknowledgement: This research work was supported by Universiti Sains Malaysia, Short-Term Grant with Project No: 304/PELECT/6315776.

REFERENCES

[1] O. Abdelrahman, T. Abdelrahman, H. Mostafa, M. Hossam, Z. Ahmed, G. Mostafa, A. Muna, M. Hossam, S. Mohamed, "Advancements in photovoltaic technology: a comprehensive review of recent advances and future prospects," *Energy Conversion and Management: X*, vol. 26, 2025, doi: 10.1016/j.ecmx.2025.100952.

[2] A. Lakhouit, N. Alhathlaul, C. ElMokhi, H. Hachimi, "Assessing the environmental impact of PV emissions and sustainability challenges," *Sustainability*, vol. 17, no.7, p. 2842, 2025, doi: 10.3390/su17072842.

[3] A. Olabi, K. Elsaid, K. Obaideen, M. Abdelkareem, H. Rezk, T. Wilberforce, H. Maghrabie, E. Sayed, "Renewable energy systems: comparisons, challenges and barriers, sustainability indicators, and the contribution to UN sustainable development goals," *International Journal of Thermofluids*, vol. 20, 2023, doi: 10.1016/j.ijft.2023.100498.

[4] H. Kumba, O. Olanrewaju, R. Pasipamire, "Integration of renewable energy technologies for sustainable development in South Africa: a focus on grid-connected PV systems," *Energies*, vol. 17, no. 12, p. 2823, 2024, doi: 10.3390/en17122823.

[5] M. Hasan, S. Hossain, M. Mofijur, Z. Kabir, I. Badruddin, T. Khan, E. Jassim, "Harnessing solar power: a review of photovoltaic innovations, solar thermal systems, and the dawn of energy storage solutions," *Energies*, vol. 16, no. 18, p. 6456, 2023, doi: 10.3390/en16186456.

[6] O. Bamisile, C. Acen, D. Cai, Q. Huang, I. Staffell, "The environmental factors affecting solar photovoltaic output," *Renewable and Sustainable Energy Reviews*, vol. 208, 2025, doi: 10.1016/j.rser.2024.115073.

[7] E. Sepúlveda-Oviedo, "Impact of environmental factors on photovoltaic system performance degradation," *Energy Strategy Reviews*, vol. 59, 2025, doi: 10.1016/j.esr.2025.101682.

[8] M. Hariri, M. Desa, S. Masri, M. Zainuri, "Grid-connected PV generation system—components and challenges: a review," *Energies*, vol. 13, no. 17, p. 4279, 2020, doi: 10.3390/en13174279.

[9] A. Almutairi, A. Abo-Khalil, K. Sayed, N. Albagami, "MPPT for a PV grid-connected system to improve efficiency under partial shading conditions," *Sustainability*, vol. 12, no. 24, p. 10310, 2020, doi: 10.3390/su122410310.

[10] A. Azar, A. Abed, F. Abdulmajeed, I. Hameed, N. Kamal, A. Jawad, A. Abbas, Z. Rashed, Z. Hashim, M. Sahib, I. Ibraheem, R. Thabit, "A new nonlinear controller for the maximum power point tracking of photovoltaic systems in micro grid applications based on modified anti-disturbance compensation," *Sustainability*, vol. 14, no. 17, p. 10511, 2022, doi: 10.3390/su141710511.

[11] E. Isen, A. F. Bakan, "Highly efficient three-phase grid-connected parallel inverter system," *Journal of Modern Power Systems and Clean Energy*, vol. 6, no. 5, pp. 1079–1089, 2018, doi: 10.1007/s40565-018-0391-7.

[12] P. Gawhade, A. Ojha, "Recent advances in synchronization techniques for grid-tied PV system: A review," *Energy Reports*, vol. 7, pp. 6581-6599, 2021, doi: 10.1016/j.egyr.2021.09.006.

[13] B. Bendib, H. Belmili, F. Krim, "A survey of the most used MPPT methods: Conventional and advanced algorithms applied for photovoltaic systems," *Renewable and Sustainable Energy Reviews*, vol. 45, pp. 637-648, 2015, doi: 10.1016/j.rser.2015.02.009.

[14] K. Tawfiq, P. Sergeant, A. Mansour, "Comparative analysis of space vector pulse-width modulation techniques of three-phase inverter to minimize common mode voltage and/or switching losses," *Mathematics*, vol. 12, no. 18, p. 2832, 2024, doi: 10.3390/math12182832.

[15] S. Kulkarni, D. Gaonkar, "An investigation of PLL synchronization techniques for distributed generation sources in the grid-connected mode of operation," *Electric Power Systems Research*, vol. 223, p. 109535, 2023, doi: 10.1016/j.epsr.2023.109535.

[16] W. Alhosaini, M. Aly, E. Ahmed, A. Shawky, "Optimized grid-connected three-phase photovoltaic inverter system using cascaded FOPIT-FOPI fractional controller," *Energy Reports*, vol. 13, 2025, doi: 10.1016/j.egyr.2025.02.055.

[17] C. Emeghara, S. Mahajan, A. Arzani, "Two-stage photovoltaic system with a high-gain fifth-order boost converter," *e-Prime - Advances in Electrical Engineering, Electronics and Energy*, vol. 13, 2025, doi: 10.1016/j.prime.2025.101038.

[18] C. Aouadi, A. Abouloifa, M. Aourir, I. Lachkar, B. Tighazouane, Y. Boussairi, "Nonlinear control of double stage three-phase grid-connected photovoltaic systems," *IFAC-PapersOnLine*, vol. 55, no. 12, 2022, doi: 10.1016/j.ifacol.2022.07.365.

[19] E. Khawla, D. Chariag, L. Sbita, "A control strategy for a three-phase grid connected PV system under grid faults," *Electronics*, vol. 8, no. 8, p. 906, 2019, doi: 10.3390/electronics8080906.

[20] L. Lam, T. Phuc, N. Hieu, "Simulation models for three-phase grid connected pv inverters enabling current limitation under unbalanced faults", *Engineering, Technology & Applied Science Research*, vol. 10, no. 2, pp. 5396–5401, 2020, doi: 10.48084/etasr.3343.

[21] X. Fu, Q. Fu, W. Tang, "Grid connection technique based on μ theory for a two-stage PV structure," *IET Power Electronics*, vol. 12, pp. 1545-1553, 2019, doi: 10.1049/iet-pel.2018.5941.

[22] H. Hadi, A. Kassem, H. Amoud, S. Nadweh, "Improve power quality and stability of grid-connected PV system by using series filter," *Heliyon*, vol. 10, no. 21, 2024, doi: 10.1016/j.heliyon.2024.e39757.

[23] M. Hariri, M. Salem, M. Jamil, M. Abdullah, M. Desa, "Modeling and analysis of 100 kW two-stage three-phase grid-connected PV generation system under absurd atmospheric and grid disturbances," *PLoS One*, vol. 20, no. 6, 2025, doi: 10.1371/journal.pone.0323269.

[24] J. Li, D. Xiao, H. Lei, T. Zhang, T. Tian, "Using cuckoo search algorithm with Q-learning and genetic operation to solve the problem of logistics distribution center location," *Mathematics*, vol. 8, no. 2, 2020, doi: 10.3390/math8020149.

[25] T. Mariprasath, C. Basha, B. Khan, A. Ali, "A novel on high voltage gain boost converter with cuckoo search optimization based MPPT Controller for solar PV system," *Scientific Reports,* vol. 14, p. 8545, 2024, doi: 10.1038/s41598-024-58820-2.

[26] J. Riba, M. Moreno-Eguilaz, S. Bogarra, A. Garcia, "Parameter identification of DC-DC converters under steady-state and transient conditions based on white-box models," *Electronics*, vol. 7, no. 12, 2018, doi: 10.3390/electronics7120393.

[27] B. Hasaneen, A. Mohammed, "Design and simulation of DC/DC boost converter," 2008 12th International Middle-East Power System Conference, 2008, doi: 10.1109/MEPCON.2008.4562340.

[28] M. Kumar, S. Dalai, R. Thakur, G. Panda, "Three-phase voltage source inverter: design and development with 180° mode of conduction,'' Proceedings of Third International Symposium on Sustainable Energy and Technological Advancements, 2024, doi: 10.1007/978-981-97-7018-2_39.

[29] Muhammad Rashid, *Power Electronics: Circuits, Devices, and Applications*, Pearson Prentice Hall, 2004.

[30] N. Mooniarsih, S. Masri, M. Hafeez, A. Hiendro, "A grid-connected photovoltaic interface system for delivering active and reactive powers," *International Journal of Power Electronics and Drive Systems*, vol. 9, no. 3, p. 1140, 2018, doi: 10.11591/ijpeds.v9.i3.pp1140-1146.

[31] S. Chatterjee, S. Chatterjee, "Simulation of synchronous reference frame PLL based grid connected inverter for photovoltaic application," 1st Conference on Power, Dielectric and Energy Management at NERIST, 2015, doi: 10.1109/ICPDEN.2015.7084493.

[32] A. Rizqiawan, P. Hadi, G. Fujita, "Development of grid-connected inverter experiment modules for microgrid learning," *Energies*, vol. 12, no. 3, pp. 1–16, 2019, doi: 10.3390/en12030476.

[33] S. Golestan, M. Ramezani, J. M. Guerrero, M. Monfared, "dq-frame cascaded delayed signal cancellation- based PLL: analysis, design, and comparison with moving average filter-based PLL," *IEEE Transactions on Power Electronics*, vol. 30, no. 3, pp. 1618-1632, 2015, doi: 10.1109/TPEL.2014.2315872.

[34] R. Mastromauro, "Grid synchronization and islanding detection methods for single-stage photovoltaic systems," *Energies*, vol. 13, no. 13, p. 3382, 2020, doi: 10.3390/en13133382.

[35] A. Manjula, A. Babu, "Grid-connected double-stage PV system with space vector PWM inverter and MPPT," *International Journal of Applied Power Engineering,* vol. 13, no. 4, 2024, doi: 10.11591/ijape.v13.i4.pp900-908.

[36] K. Boutaghane, N. Bennecib, M. Benidir, H. Benbouhenni, I. Colak, "Performance enhancement of a three-phase grid-connected PV inverter system using fractional-order integral sliding mode controls," *Energy Reports*, vol. 11, 2024, doi: 10.1016/j.egyr.2024.03.049.

[37] A. Eltamaly, Z. Almutairi, "Synergistic coordination between PWM inverters and DC-DC converters for power quality improvement of three-phase grid-connected PV systems," *Sustainability*, vol. 17, no. 8, p. 3748, 2025, doi: 10.3390/su17083748.